J Fluoresc (2011) 21:1265–1279
DOI 10.1007/s10895-010-0809-8

ORIGINAL PAPER

# On the Photophysics of 3,5,6-Trichlorosalicylic Acid: Spectroscopic Study Combined with Hartree-Fock and Density Functional Theory Calculations

**Bijan Kumar Paul · Anuva Samanta · Nikhil Guchhait**

Received: 9 April 2010 / Accepted: 29 December 2010 / Published online: 18 January 2011


**Abstract** The present contribution reports a detailed photophysical study of a simple salicylic acid derivative viz., 3,5,6-Trichlorosalicylic acid (TCSA) based on steady state absorption, emission and time-resolved emission spectroscopy. Anomalous "dual" emission coupled with a large Stokes shift and negligible solvent polarity dependence marks the spectroscopic signature for Excited State Intramolecular Proton Transfer (ESIPT) reaction. Variation of medium polarity and pH of the medium have been implemented as fruitful tools to decipher the photophysics of TCSA. Quantum chemical calculation by *ab initio* Hartree-Fock and Density Functional Theory methods yields consistent results to follow experimental findings with distinct illustration of the inoperativeness of GSIPT reaction as well as occurrence of ESIPT process. A rigorous comparison of our experimental and theoretical measurements of TCSA with the parent compound salicylic acid, 5-chlorosalicylic acid and 3,5-dichlorosalicylic acid reveals the impact of chlorine substitution on the photophysics of the studied molecular systems with simultaneous exploration of the complexities induced in TCSA with respect to salicylic acid.

**Keywords** 3,5,6-Trichlorosalicylic acid · ESIPT · Intramolecular hydrogen bond · HF · DFT · Absorption · Fluorescence

B. K. Paul · A. Samanta · N. Guchhait (✉)
Department of Chemistry, University of Calcutta,
92 A. P. C. Road,
Calcutta 700009, India
e-mail: nguchhait@yahoo.com

## Introduction

Ever since the first report of Excited State Intramolecular Proton Transfer (ESIPT) reaction by Weller [1] in the middle of the last century, the field of photochemistry has witnessed an explosive evolution of research surrounding this phenomenon. A look on the diverse range of applications of ESIPT probes/phenomenon stands strong in support of this august development. The unique four-level photophysical scheme characteristic of proton transfer (PT) reaction normally allows the total exclusion of self-absorption together with a large Stokes shifted emission (i.e. rupture of mirror image symmetry between absorption and emission spectra since the absorbing (E→E*) and emitting (K*→K) species are largely different in respect of their electronic structure and stability) whereby indulging in its many faceted application as proton transfer laser [2, 3], photopatterning media [4], white-light emitting diode [5], UV filters [6] and so forth. Also application of ESIPT probes as molecular reporters for extracting valuable information from complex biological, biomimicking and various supramolecular systems have long been recognized to commendable fruition [7]. Quite recently the photoswitchabilty of ESIPT molecules (changeover between enol and keto tautomers) has been capturing attention because of their viable application towards the development of ultrahigh-density erasable optical memory [8]. ESIPT probes happen to constitute a splendid avenue for fruitful execution of the design of target molecules which allow switching and tuning of luminescence properties by modulating the mode of molecular packing without chemical alterations of the molecule, and this strategy is being recognized as a strongly promising candidate in

future technology of devising strategies like proton-transfer laser, white-light emitting devices *et cetera* [8].

Although the basics of ESIPT process have received a great maturity through the massive volume of research works inclined along the subject line [1–20], it happens to come up with striking challenges even today, both theoretically and experimentally. This is primarily because of the inherently complicated physical (e.g., quantum nature) and chemical (cleavage and formation of H-bond and subsequent nuclear rearrangement with inversion in the thermodynamic stability) nature of the process. Such complexities have always acted in the direction of affording colossal impetus to the study of ESIPT process even in some of very simple and archetype systems, as such that a huge volume of experimental and theoretical research has been centered on salicylic acid (SA) and related compounds over the span of past few years [9–21].

Although quite a few reports appear in the literature on the study of substitution effect on ESIPT of SA, but those are focused on substitution at the intramolecular hydrogen bond (IMHB) ring site mainly [11, 17–20]. Studies intending to delve into the effects of substitution on the aromatic nucleus have, however, been sporadically discussed [22]. The present programme is thus designed to look into the effect of chlorine substitution on the benzene ring on the photophysics of SA with a target to have positive impact in the process of filling in this gap. The present contribution is indeed a part of our series of spectroscopic works performed with a view to establish the influence of chlorine substitution in the benzene nucleus on the photophysics of SA (with particular emphasis on the ESIPT process) and is following to two recent reports from our group [23, 24]. In the present work, the various species present in the ground and excited states of TCSA are characterized by a thorough spectroscopic investigation including variation of pH and solvent polarity. Furthermore, computational results at Hartree-Fock (HF) and Density Functional Theory (DFT) levels are implemented to correlate the experimental findings. In essence, the spectroscopic observations with TCSA have been interpreted on the lexicon of spectral properties of the parent molecule SA. Finally, the photophysical findings with TCSA have been subjected to rigorous comparison with those of its parent molecule SA, and the monochloro (5-chlorosalicylic acid [23]) and dichloro (3,5-dichlorosalicylic acid [24]) counterparts with a view to execute the attempt of exploring the influence of chlorine substitution on the aromatic benzene nucleus on ESIPT barrier, intramolecular hydrogen bond (IMHB) energy and overall photophysics of SA, the benchmark ESIPT molecule.

## Experimental

### Materials

3,5,6-Trichlorosalicylic acid (TCSA) was purchased from SRL, India and was used after recrystallization twice from ethanol. The purity of the sample was established on TLC plate before use. Spectroscopic grade solvents such as methylcyclohexane (MCH), acetonitrile (ACN), tetrahydrofuran (THF), dioxane (DOX), dichloromethane (DCM), chloroform ($CHCl_3$), n-butanol (BuOH), iso-prpanol (iPrOH), methanol (MeOH), ethanol (EtOH), dimethylsulfoxide (DMSO) purchased from Spectrochem, India were used after proper distillation. The purity of the solvents was also verified by running their spectra in the studied wavelength range. Sulfuric acid ($H_2SO_4$), sodium hydroxide (NaOH) from E-Merck and triethylamine (TEA), trifluoroacetic acid (TFA) from Spectrochem, India were used as received. Triple distilled water was used for preparing aqueous solutions.

### Apparatus and Methods

The absorption and emission spectra were acquired on Hitachi UV-Vis U-3501 spectrophotometer and Perkin-Elmer LS-50B fluorimeter, respectively. In all measurements the sample concentration was maintained in the range $\sim 10^{-6}$ M in order to avoid aggregation and reabsorption effects. Only freshly prepared solutions were used for spectroscopic studies and all experiments have been carried out with air-equilibrated solutions at ambient temperature (300 K) unless otherwise specified. Fluorescence quantum yield ($\Phi_f$) was determined by considering β-naphthol as the secondary standard ($\Phi_f$= 0.23 in methylcyclohexane) [25–27] using the following equation:

$$\frac{\Phi_S}{\Phi_R} = \frac{A_S}{A_R} \times \frac{(Abs)_R}{(Abs)_S} \times \frac{n_S^2}{n_R^2} \quad (1)$$

where $A$ terms denote the fluorescence area under the curve, *"Abs"* denote absorbance, $n$ is the refractive index of the medium and $\Phi$ is the fluorescence quantum yield and subscripts *"S"* and *"R"* stand in recognition of the respective parameters for the studied sample and reference, respectively.

Fluorescence lifetimes were obtained from time-resolved intensity decays by the method of Time Correlated Single-Photon Counting (TCSPC) using a nanosecond diode laser at 340 nm (IBH, nanoLED-07)

as the light source to trigger the fluorescence of TCSA, and TBX-04 as the detector, and the signals were collected at the magic angle of 54.7°. The decays were deconvoluted on Data Station v-2.5 decay analysis software. The excellence of the fits was judged by $\chi^2$ criteria and visual inspection of the residuals of the fitted function to the data. Mean (average) fluorescence lifetimes were calculated using the following equation [7, 9]:

$$\langle \tau_f \rangle = \sum_i \alpha_i \tau_i^2 \Big/ \sum_i \alpha_i \tau_i \qquad (2)$$

in which $\alpha_i$ is the pre-exponential factor corresponding to the ith decay time constant, $\tau_i$.

### Computational Procedures

The ground state structural calculations for various possible conformations of TCSA were computed at the Hartree-Fock (HF) and Density Functional Theory (DFT) levels (B3LYP/6-311 G**) using GAUSSIAN 03W suite of programmes [28]. The ground state intramolecular proton transfer (GSIPT) curves were evaluated using the energies of B3LYP/6-311 G** fully optimized geometry at fixed $O_d$-H (Chart 1) distances over the range 0.94–1.84 Å [12, 15, 16, 25–28].

The excited state potential energy curves (PECs) were obtained by calculating the Franck-Condon transition energies for the B3LYP/6-311 G** ground state optimized structures at fixed $O_d$-H distances at the TDDFT/6-311 G** level. The Franck-Condon curves for the proton transfer process were obtained by adding the TDDFT/6-311 G** excitation energies to the corresponding GSIPT curves [12, 15, 16, 25–28]. This type of approach has been successfully reported in several recent papers for studying ESIPT reaction [12, 15, 16, 25–29]. However, several other methods are also reported for elucidation of PES for the proton transfer reaction [29]. The CASSCF study on the ESIPT reaction of 2-(2′-hydroxyphenyl) benzotriazole predicts true reaction path through a twisted geometry [28]. Sobolewski et al. employed successfully CASSCF and CIS electronic structure method to study proton transfer in 7-hydroxy-1-indanone and related compounds and they have compared the results of CASSCF and CASPT2 with TDDFT method [12b]. The strength of the IMHB ($E_{IMHB}$) was estimated from the energy difference between fully optimized molecular structures of the E-form and the non-hydrogen bonded form (with the –OH or –COOH group rotated 180° away from the hydrogen bonded conformation) [12, 15, 16, 25–31].

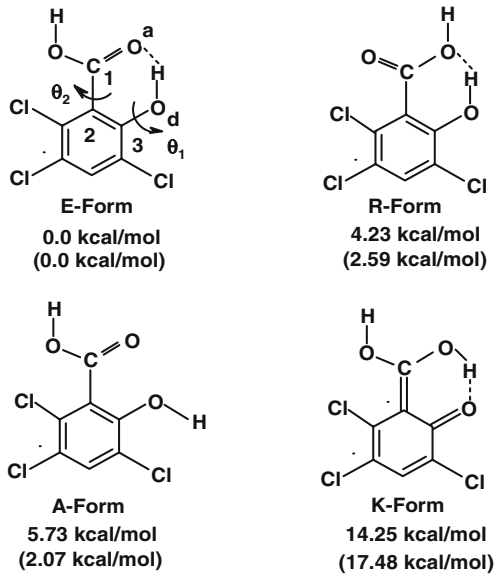


**Chart 1** Schematic presentation of computed ground state low energy structures and K-form of TCSA and their energies at DFT/6-311G** and HF/6-311G** (in parenthesis) levels. Energies are relative to the E-form

## Results and Discussion

### Absorption Spectra

The absorption spectra of TCSA recorded in different solvents are displayed in Fig. 1 and the corresponding spectroscopic parameters are collected in Table 1. The absorption profile beholds the distinct appearance of two humps in all solvents—the higher energy hump being centered at ~300 nm while the lower energy main absorption band is located in the range 320–330 nm. The assignment of the observed spectral features, of course, rests on a comparison with the parent molecule salicylic acid (SA). Bisht et al. [25] studied the excitation spectra of SA (monomer) under supersonic nozzle expansion conditions and found the $S_1 \leftarrow S_0$ transition to have its origin at 335.35 nm and 311.52 nm and subsequently ascribed the bands to the E-form and R-form of SA (Chart 1), respectively. A direct analogy therefore drives us to attribute the higher energy (~300 nm) and the lower energy (320–330 nm) bands of TCSA respectively to the R- and E-forms (Chart 1) of TCSA. The absorption profile thus reflects the greater stability of the intramolecularly hydrogen bonded E-form. However, the appearance of an apparently broad spectrum is a commonly encountered characteristic of condensed phase spectra and the responsibility might well be entrusted on the extensive solute-solvent interactions occurring within the system [23, 24,

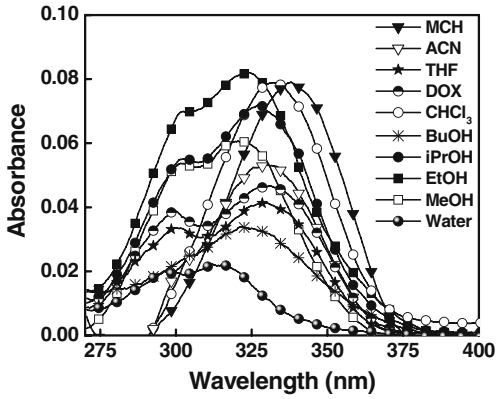


**Fig. 1** Absorption spectra of TCSA in different solvents as indicated in the inset

32]. Similar broad spectral shape was also noted for SA in condensed phase. A slight blue shift observed in water ($\lambda_{abs}$~295 nm) is perceived based on the idea of deprotonation of the carboxyl group leading to the formation of an anionic species, since deprotonation of carboxyl group is known to give rise to blue shifted absorption [21, 22, 25, 33]. The absorption spectral properties of TCSA in various solvents when compared to those of its parent molecule SA and the monochloro (5ClSA) [23] and dichloro (3,5DCSA) [24] counterparts, reveals a more or less comprehensible red shift across the sequence SA→5ClSA→3,5DCSA→TCSA (*ca.* ~310 nm in SA vs. ~322 nm in 5ClSA vs. ~325 nm in 3,5DCSA vs. ~338 nm in TCSA in non-polar solvent MCH and ~306 nm in SA vs. ~316 nm in 5ClSA vs. ~320 nm in 3,5DCSA vs. ~330 nm in TCSA in polar aprotic solvent ACN and ~300 nm in SA vs. ~312 nm in 5ClSA vs. ~318 nm in 3,5DCSA vs. ~325 nm in TCSA in polar protic solvent MeOH). This implies that increasing number of chlorine substitution subsequently modulates the stabilization of its different energy levels, presumably in direction of relative lowering of the energy gap between HOMO (highest occupied molecular orbital) and LUMO (lowest unoccupied molecular orbital) giving rise to the comparative red shift. However, the effect is not so large in magnitude.

## Emission and Excitation Spectra

The emission profile of TCSA (Fig. 2a and b) readily arrests attention by producing interesting observations in terms of distinct dual emission coupled with a large Stokes shifted emission band in all types of solvents to register the "*spectroscopic signature*" of ESIPT reaction. The large Stokes shift is in fact an indicator of the marked difference between E- and K- forms in respect of electronic structure and stability since the emission observed in the range 460–475 nm is attributed to the K-form, whereas the weakly intense higher energy emission is coming from the locally excited R-form of TCSA (Scheme 1). The prominence of dual emission is, however, obscured in case of monitoring the emission behaviour at $\lambda_{ex}$~300 nm ($\lambda_{abs}^{max}$ of the R-form; "Absorption spectra", Fig. 2b) at the cost of appearance of a very broad spectrum. It is reasonable to assume that in this case, the emission from both the R- and K-forms is getting overlapped under the single arena of the broad spectral profile. Our spectral assignments of TCSA are, however, banked upon a strong support from a direct comparison with the emission spectral characteristics of SA. In SA also, the operation of ESIPT reaction is manifested through a large Stokes shifted emission in all types of solvents centered at 425–456 nm region together with a high energy emission band at ~350 nm coming from the R-form of SA (figures not given).

The condensed phase emission spectral properties of SA, 5ClSA, 3,5DCSA and TCSA when examined under a single

**Table 1** Spectroscopic parameters for TCSA in different solvents as obtained from absorption and emission measurements

| Solvent | Absorption maxima (nm) | | Emission maxima (nm) | | Quantum yield, $\Phi_f$ | | |
|---|---|---|---|---|---|---|---|
| | $\lambda_1$ | $\lambda_2$ | $\lambda_1$ | $\lambda_2$ | $\Phi_{E*}$[a] | $\Phi_{K*}$[a] | $\Phi_{E*}/\Phi_{K*}$ |
| MCH | – | 338 | 375 | 470 | 0.387 | 0.147 | 0.263 |
| ACN | 300 | 330 | 370 | 465 | 3.882 | 1.567 | 0.248 |
| DCM | 300 | 335 | 385 | 475 | – | – | – |
| THF | 300 | 330 | 375 | 465 | 0.596 | 3.270 | 0.018 |
| DOX | 298 | 330 | 375 | 465 | 2.033 | 2.552 | 0.0797 |
| BuOH | 300 | 325 | 375 | 460 | 0.621 | 1.321 | 0.0470 |
| iPrOH | 300 | 328 | 385 | 460 | 6.747 | 5.201 | 0.1297 |
| EtOH | 300 | 325 | – | 460 | 0.557 | 1.271 | 0.0438 |
| MeOH | 300 | 325 | 385 | 464 | 0.363 | 0.804 | 0.0045 |
| $MeOH+H^+$ | – | – | – | 467 | – | – | – |
| $MeOH+OH^-$ | – | – | – | 435 | – | – | – |
| Water | 295 | 315 | 400 | 428 | 3.758 | 0.586 | 0.6413 |

[a] $\Phi_{E*}$ are of $\times 10^{-3}$ and $\Phi_{K*}$ are of $\times 10^{-2}$ orders of magnitude

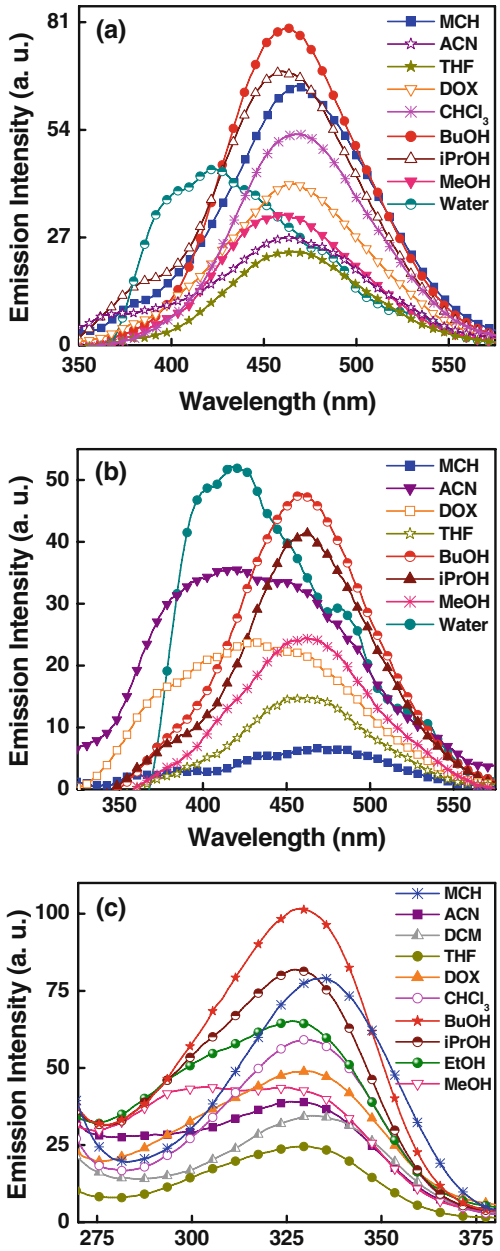


**Fig. 2** Emission spectra of TCSA in different solvents (indicated in the inset) for **a** $\lambda_{ex}$=330 nm and **b** $\lambda_{ex}$=300 nm. **c** Fluorescence excitation spectra of TCSA in different solvents ($\lambda_{em}=\lambda_{PT}$)

pavilion, a broad overview is unveiled in form of a progressive red shift along the sequence of increasing number of chlorine substituents on the benzene nucleus of the studied compounds (*ca.* ~456 nm in SA vs. ~453 nm in 5ClSA vs. ~463 nm in 3,5DCSA vs. ~470 nm in TCSA in non-polar solvent MCH and ~390 nm in SA vs. ~436 nm 5ClSA vs. ~415 nm in 3,5DCSA vs. ~465 nm in TCSA in polar aprotic solvent ACN and ~440 nm in SA vs. ~415 nm 5ClSA vs. ~422 nm in 3,5DCSA vs. ~464 nm in TCSA in polar protic solvent MeOH). The red shift, however, being relatively more conspicuously seen in cases of polar protic solvents compared to those in aprotic (nonpolar or polar aprotic) ones (*ca.* ~440 nm in SA vs. ~415 nm 5ClSA vs. ~422 nm in 3,5DCSA vs. ~464 nm in TCSA in polar protic solvent MeOH and ~404 nm in SA vs. ~421 nm in 5ClSA vs. ~450 in 3,5DCSA vs. ~460 nm in TCSA in iPrOH and ~405 nm in SA vs. ~423 nm 5ClSA vs. ~434 nm in 3,5DCSA vs. ~460 nm TCSA in BuOH). With an attention of considering only the electron withdrawing inductive effect of the chlorine substitutions the observed results seem to pose a little contradiction to an expected blue shift. Thus the present set of experimental data signals the concurrent operation of some other sort of interactions apart from only electron withdrawal by the chlorine atoms. It is, indeed, logical to assume that a conjugate impact of electron withdrawing inductive and electron donating resonance effects of the chlorine substituents play the pivotal role in governing the overall photophysics of the compounds. The lack of a steady pattern in the magnitudes of the observed spectral shifting as a function of number of substituent chlorine atoms seems to be an added support to the aforementioned postulation, since the strength of electron withdrawing inductive and electron donating resonance effects of each chlorine atom on the ESIPT framework (–COOH and –OH functional moieties) will obviously be different depending on its relative location on the aromatic nucleus. Thus, interplay of these two effects will exercise a complex impact while moving across the sequence SA→5ClSA→3,5DCSA→TCSA. Also with a view to a relatively more pronounced manifestation of the red shift in protic solvents, the solute-solvent interactions (in form of intermolecular hydrogen bond formation, dipole-dipole interaction *et cetera*) appear to put a signature on the excited state photophysics of the molecules. However, the aforementioned factors are likely to be more promising in having an impact on the excited state photophysics of the molecules since it is the relatively more polar and more energetic state. Furthermore, considering the steric factor of bulky chlorine substituents and/or an electrostatic repulsive affair between the lone electron pairs of Cl-atoms and –OH/–COOH groups might add additional complicacies. Obviously, the above discussion thus seems to advocate in favour of negating the provision of a unified explanation which can simultaneously account for all the possible interactions. Under a broad spectrum, the present study may be invoked to document that introduction of chlorine substitution on the benzene ring of SA does not impart substantially sizeable modulations of its overall photophysics, though some detectable modifications are observed.

Figure 2c reveals that the excitation spectra obtained in all solvents assayed qualitatively juxtapose well with the corresponding absorption spectra indicating that the origin of the tautomer (K-form) emission is through excitation of

**Scheme 1** Different ground and excited state species of TCSA and a simplified view of its photophysics

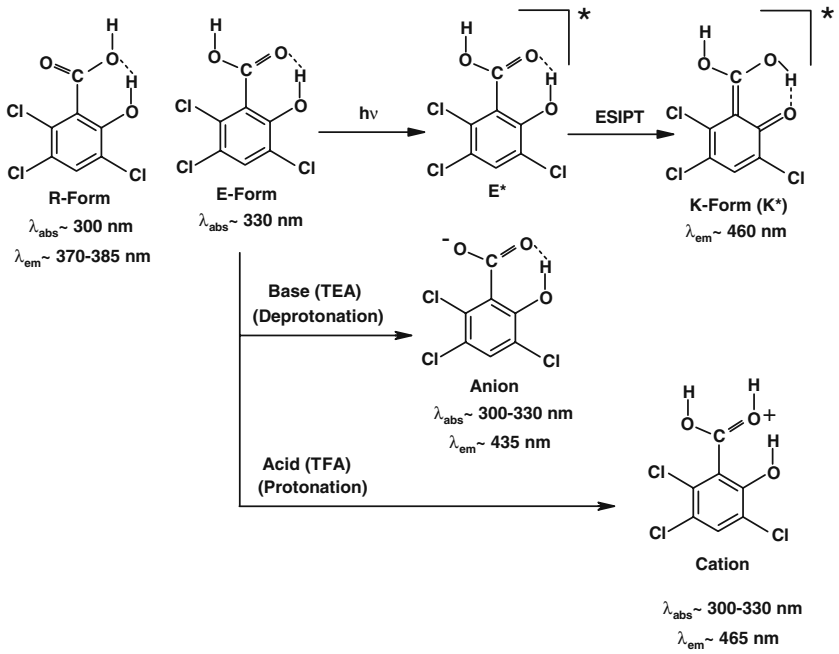


the E-form i.e. the observed phenomenon of proton transfer is exclusively an excited state affair.

## Spectral Modulations as a Function of Medium-pH

The pH variation experiments produced some interesting observations with imperative contributions to the goal of our work, i.e. to decipher the ground and excited state photophysics of TCSA. Addition of a base, NaOH to a methanolic solution of TCSA is found to result in little increment of absorbance intensity together with a remarkable broadening of the spectrum (Fig. 3a). The prototype compound SA, however, experiences a blue shift under the same experimental conditions (from $\lambda_{abs}$~300 nm in MeOH to $\lambda_{abs}$~292 nm in the presence of base) presumably because of the formation of anionic species out of deprotonation of the –COOH group [25, 33]. The extensive broadening of spectral profile in the present case renders the precise location of a similar blue shifted band quite improbable indeed. However, similar are the results for base (NaOH) treatment with 5ClSA (a blue shift of the abosorption band from $\lambda_{abs}$~312 nm in MeOH to $\lambda_{abs}$~307 nm in MeOH in the presence of base) and 3,5DCSA (from $\lambda_{abs}$~322 nm in MeOH to $\lambda_{abs}$~314 nm in the presence of base). Conversely, the application of an acid ($H_2SO_4$) to a methanolic solution of TCSA yields better resolved effects, as is displayed in Fig. 3b, in terms of decrement of intensity of the higher energy band with concomitant increment of same for the lower energy band. These observations are argued based on the idea that the presence of $H^+$ ions in the medium is necessarily to induce protonation reaction (Scheme 1) whereby lowering the population of the closed conformer (E-form) with simultaneous rise of the same of its protonated counterpart. Similar results for pH variation experiments in a polar aprotic medium, ACN (figures not given) further substantiates the

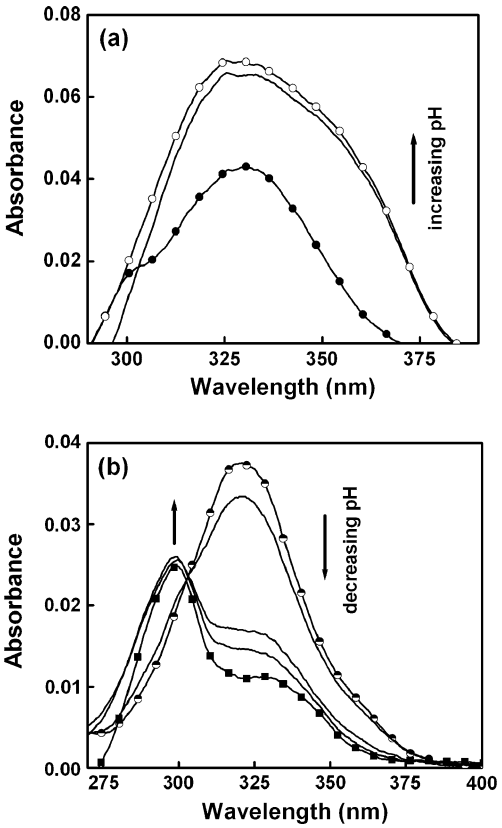


**Fig. 3** Effect of variation of pH on the absorption profile of TCSA in methanolic medium: **a** increasing pH (addition of base, NaOH) and **b** decreasing pH (addition of acid, $H_2SO_4$)

effect of decreasing the medium pH on the absorption profile of TCSA.

On the emission profile, however, differential pH of the medium resulted in some well resolved spectral modifications. As depicted in Fig. 4a, increasing the pH of a methanolic solution of TCSA resulted in a spectral blue shift (from $\lambda_{em}$~464 nm to 435 nm) with concomitant decrement of intensity and somewhat broadening of the spectrum. Whereas by decreasing the pH we observed modifications of spectral features in quite a reverse pattern i.e. a slight intensity enhancement coupled with a slight red shift ($\lambda_{em}$~464 nm to 467 nm; Fig. 4b). Such consistent shifting of emission maxima as a function of medium-pH seems to comply with the proposition of protonation and deprotonation reactions, respectively in acidic and alkaline pH (Scheme 1). Similar results are found for pH variation experiments in a polar aprotic medium, ACN (figures not given). Also these findings are consistent with literature reports [9, 12, 25, 33]. It is noteworthy to mention here that very similar observation was found with SA during pH variation experiments. Treatment with a base (TEA) results in blue shift of the emission maxima of SA from ~456 nm in MCH to ~423 nm. This ~423 nm emission band is formally attributed to the anionic species formed upon deprotonation of –COOH group of SA. Whereas addition of an acid (TFA) in MCH solution of SA is found to suppress the tautomer (PT) emission (~456 nm) with subsequent enhancement of the higher energy emission from the R-form (~375 nm) (figures not given). Therefore, a direct comparison of TCSA with its parent molecule SA affords reasonable qualitative support to sustain our present findings and interpretations. Although the comparison with SA, especially in respect of spectral response to variation of medium pH, is not quite easy since the photophysics of TCSA carries with it additional complicacies by virtue of the presence of the chlorine atoms. Depending on the location of the chlorine atoms on the aromatic nucleus with respect to –OH and –COOH functional moieties, relative contributions from their electron withdrawing inductive effect and electron donating resonance effect will vary to add further complicacy to the photophysics of TCSA. However, with the monochloro (5ClSA) and dichloro (3,5DCSA) counterparts, qualitatively similar results are obtained, e.g. with 5ClSA the emission profile exhibits a blue shift (from $\lambda_{em}$~415 nm to $\lambda_{em}$~407 nm) upon base treatment on a methanolic solution and a relative red shift upon acid treatment ($\lambda_{em}$~415 nm to $\lambda_{em}$~435 nm) [23] and with 3,5DCSA base treatment causes a blue shifted emission from $\lambda_{em}$~422 nm to $\lambda_{em}$~418 nm and the red shift following acid treatment is from $\lambda_{em}$~422 nm to $\lambda_{em}$~458 nm [24]. That the results of variation of medium pH are qualitatively similar over the entire sequence SA→5Cl-SA→3,5DCSA→TCSA advocates for generalization of the findings and their interpretations.

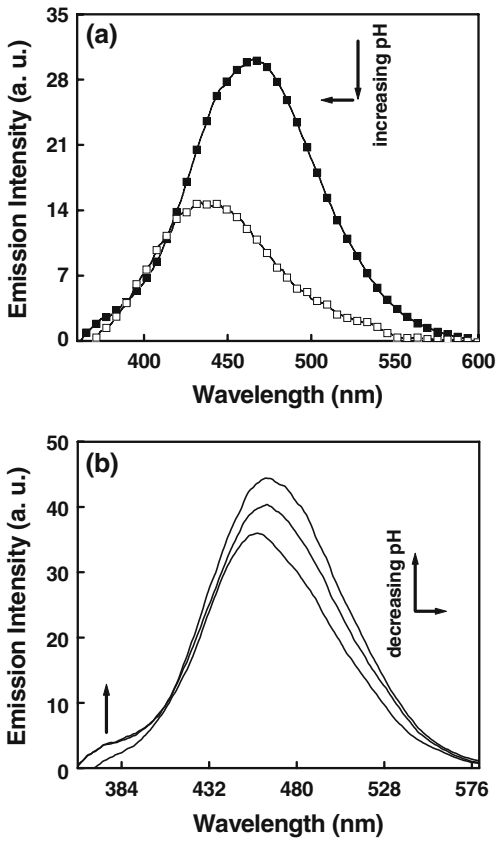


**Fig. 4** Effect of variation of pH on the emission profile of TCSA in methanolic medium ($\lambda_{ex}$=325 nm): **a** increasing pH (addition of base, NaOH) and **b** decreasing pH (addition of acid, $H_2SO_4$)

Although a comparison of absorption and emission spectral properties between SA and TCSA qualitatively explores the influence of chlorine substitution on benzene nucleus, a more rigorous comparison having 5ClSA [23] and 3,5DCSA [24] being included in the queue, however, failed to mark the effect with equally conspicuous resolution. This is not surprising with a view to the common characteristics of condensed phase spectra i.e., reasonably broad profiles under which it is not possible to detect any minor shifting of spectral (absorption or emission) band maxima positions. Consequently, on going from 5ClSA to 3,5DCSA to TCSA we found it difficult to locate any precise difference in spectral features as an outcome of incorporation of additional chlorine atoms in terms of absorption or emission maxima positions, subject to the present experimental conditions and findings. Qualitatively the results are consistent for the four compounds, but a thorough quantitative comparison is rendered obscured by the appreciable broadening of spectral profiles. Also such observations indicate that the event of chlorine substitution on the benzene nucleus impart some qualitative modula-

tions of the photophysics of SA but leading to no drastic modifications of its overall photophysics. At the same time, the process of a thorough comparison along the sequence SA→5ClSA→3,5DCSA→TCSA was rendered increasingly cumbersome and hence difficult as we marched across the sequence, as discussed in previous sections. This seems to be a repercussion of the relatively increasing complexities induced by the increasing number of chlorine substitutions coming into play as a result of a complicated interplay of electron withdrawing inductive effect and electron donating resonance effect of chlorine substitution depending on its position on the aromatic nucleus. Additionally, the number, nature and relative positions (with respect to each other in the molecular framework) of substitutions will also exert an impact on solute-solvent interactions. Under conditions of condensed phase spectral measurements such solute-solvent interactions will in turn lead to subtle modulations of ground and excited state properties such as radiative and nonradiative decay rates, quantum yields and so forth [24].

## Fluorescence Quantum Efficiency and Excited State Fluorescence Lifetime

Table 1 lists the fluorescence quantum yields of TCSA in solvents of different polarities as measured relative to recrystallized β-naphthol using equation 1. The high magnitude of quantum yields for the red shifted emission probably points towards a greater transition cross-section of the K*-form. Later on we found that the computed oscillator strength for K*-form is higher compared to that of the E*-form. The low computed oscillator strength for the E*-form is probably due to $n\pi^*$ nature of the $S_1$ state. The probability of E* emission should be small as ESIPT reaction is inherently ultrafast in nature and the oscillator strength for the $S_1 \leftarrow S_0$ transition of the E* state is low. Furthermore, that the calculated values for $\Phi_{E^*}/\Phi_{K^*}$ is relatively higher for nonpolar and aprotic solvents than protic solvents and the quantum yield values retain a descending trend with increasing H-bond forming ability of the solvents (Table 1) is, by analogy with similar studied systems, connected to the opening up of nonradiative decay routes operating via intermolecular H-bonds formed between solute (TCSA) and solvents [9, 12, 25, 33, 34].

Now, in order to accomplish another major perspective of our present investigation we have compared the fluorescence quantum yields of TCSA with those of 5ClSA [23] and 3,5DCSA [24] and found a detectable lowering of the values for TCSA. Keeping an analogy with our previous reports, such lowering of fluorescence yields seems attributable to the enhanced degree of solute-solvent interactions (in form of dipole-dipole interactions, intermolecular H-bonding and so forth) in TCSA contributing to opening up of non-radiative deactivation channels. Such strengthening of radiationless decay routes is probably manifested in the excited state fluorescence lifetimes of TCSA also. From 5ClSA to 3,5DCSA a distinct increase in nonradiative decay rates in different solvents was observed [24], whereas the extension of the results to TCSA was crumpled by the very fast fluorescence lifetime of TCSA falling beyond the measuring limit of the instrument in all solvents except water. As a whole, such ultrafast excited state fluorescence lifetime is nothing but a beautiful corroboration of our proposition of an ultrafast ESIPT reaction in TCSA, which also reinforces the theoretical findings of a vanishingly small energy-barrier for ESIPT in the $S_1$ surface (Fig. 5, "Potential energy surfaces: GSIPT and ESIPT curves" section below). Although the exception for the case of aqueous TCSA solution (i.e. a detectable lifetime) is a bit surprising, but it seems reasonable to think that in aqueous phase the observed lifetime is actually a combined manifestation of the lifetimes of various species coexisting in the solution. Given the high degree of polarity ($E_T(30)$=63.1), dielectric constant ($\varepsilon$=80) and efficient H-bonding ability ($\alpha$=1.17, $\beta$=0.18 on Kamlet-Taft scale [35]) of water it is not surprising to consider the coexistence of various intermolecular H-bonded species, anionic species etc. in the aqueous solution. Such proposition is self-authenticated upon observing the differential absorption and emission spectral properties of the molecule in water with respect to those in other media ("Absorption spectra" and "Emission and excitation spectra", Figs. 1 and 2). Again further support comes during fitting of the raw data when only a complicated triexponential fit was found to

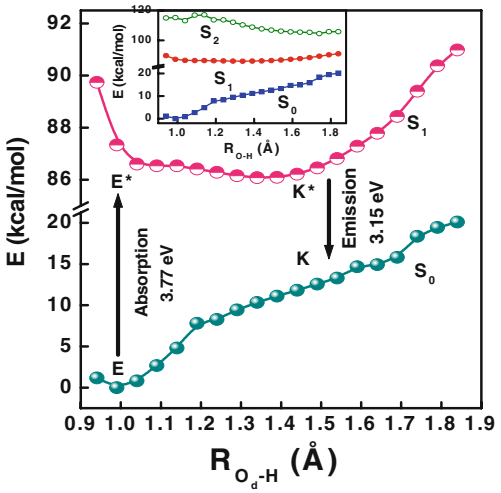


**Fig. 5** Plot of energy (kcal/mol) vs. $O_d$-H coordinate (Å). GSIPT curve ($S_0$) and ESIPT Franck-Condon curves ($S_1$) for TCSA as computed at DFT//B3LYP/6-311G** and TD-DFT//B3LYP/6-311G** levels, respectively. Inset shows a combined view of the PECs for $S_0$, $S_1$ and $S_2$ states

produce an acceptable fit with reasonable value of $\chi^2$= 0.96: $\alpha_1$=0.04, $\alpha_2$=0.04, $\alpha_3$=99.92 and $\tau_1$=1.47 ns, $\tau_2$= 6.66 ns, $\tau_3$=2.92×$10^{-3}$ ns and $<\tau_f>$=3.017 ns.

## Computational Results

### *Structures and Energies*

The conformational landscapes of TCSA are explored in the electronic ground state by HF/6-311G** and DFT/B3LYP/6-311G** methods to achieve the first insight into the phenomenon of ESIPT in TCSA. The optimized structural parameters for the E- and K-forms are collected in Table 2. Out of all possible conformers of TCSA, the E-form is predicted to be the most stable ground state form (Chart 1) as expected given the extra stabilization gained from the intramolecular hydrogen bond (IMHB).

### *Structural and Electronic Changes Associated with ESIPT*

Table 2 shows the optimized parameters for the ground (GS) and excited state (ES) geometries of TCSA calculated at HF/6-311G** level of theory. Lengthening of the $O_d$-H bond from 0.953 Å (GS) to 0.966 Å (ES) and shortening of $O_d$...$O_a$ distance from 2.564 Å to 2.525 Å together with elongation of ∠$O_d$...H...$O_a$ angle from 142.279° to 144.804° as a result of transition from ground to excited state are the consistent structural changes to be encountered in course of translocation of the proton from –OH to –COOH group following photoexcitation. Also that the $O_d$...$O_a$ distance and ∠$O_d$...H...$O_a$ angle for the K-form are closer to the corresponding excited state parameters of the E-form (E*) is an indication pointing towards ESIPT reaction.

Photoexcitation of TCSA is necessarily to impart some significant modification of the electronic charge density on the heavy atoms of the molecule, a repercussion of which is the operation of the ESIPT reaction. Thus, quite obviously a close inspection of the charge distribution over the atoms (particularly the atoms constituting the ESIPT site) will open another window to look into the process. The increase of negative charge density on O-atom of –COOH group (−0.531 in GS to −0.537 in ES) together with a decrease of the same on O-atom of –OH group (−0.431 in GS to −0.404 in ES) (computed at HF/6-311G** level according to Mulliken scheme) as an outcome of excitation from GS to ES, is along the line of translocation of the proton up on the excited surface. In case of SA, at the same level of calculation, the negative charge increment at O-atom of acid group is from −0.524 in GS to −0.553 in ES and the decrement at the O-atom of OH group is from −0.451 in GS to −0.431 in ES. A thorough comparison among SA, 5ClSA, 3,5DCSA and TCSA reveals that the numerical magnitude of the decrease in calculated negative charge density at the donor O-atom (OH group) follows the trend: SA (0.02)>5ClSA (0.019)>3,5DCSA (0.017)>TCSA (0.027). This result also advocates for the efficiency and applicability of the presently employed level of theory for calculation of electronic charge density in the studied ESIPT molecular systems. However, in case of increase of negative charge density at the acceptor O-atom (acid group) it is found to be greater in SA than in TCSA, but in course of a complete comparison along the sequence, complexities are revealed: SA (−0.029)>5ClSA (−0.027)≈3,5DCSA (−0.027)<TCSA (−0.006). Such deviations in numerical magnitudes of these charge distributions are found to follow, qualitatively, a trend along the sequence SA→5Cl-SA→3,5DCSA, but with incorporation of TCSA in the

**Table 2** Optimized ground and excited state structural parameters for TCSA relevant to ESIPT reaction as obtained from calculations at HF and CIS levels using 6-311G** basis set and DFT level using B3LYP hybrid functional and 6-311G** basis set

| Parameters | HF level | | | DFT level (Ground state) | |
|---|---|---|---|---|---|
| | E-form | | K-form | | |
| | Ground state | Excited state | Ground state | E-form | K-form |
| $O_d$-H | 0.953 | 0.966 | 1.600 | 0.990 | 1.60 |
| H...$O_a$ | 1.703 | 1.713 | 0.977 | 1.612 | 1.012 |
| $O_a$-$C_1$ | 1.198 | 1.213 | 1.281 | 1.229 | 1.301 |
| $C_1$-$C_2$ | 1.493 | 1.439 | 1.403 | 1.482 | 1.414 |
| $C_2$-$C_3$ | 1.409 | 1.448 | 1.459 | 1.429 | 1.475 |
| $C_3$-$O_d$ | 1.313 | 1.290 | 1.222 | 1.326 | 1.253 |
| $O_d$...$O_a$ | 2.564 | 2.525 | 2.466 | 2.503 | 2.509 |
| ∠$O_d$...H...$O_a$ | 142.279 | 144.804 | 145.236 | 147.314 | 146.921 |
| ∠$C_2$-$C_3$-$O_d$ | 124.538 | 121.458 | 123.368 | 123.697 | 123.525 |
| ∠H...$O_a$-$C_1$ | 104.443 | 101.375 | 109.769 | 103.360 | 108.329 |
| Dipole moment (Debye) | 1.798 | 1.903 | 3.644 | 1.822 | 3.478 |

queue complexities are apparently increased. We presume that this is a reflection of the complicated influence on the overall photophysics of SA of three chlorine substitutions. With TCSA as the present case study situations are endowed with even more complexities with a view to the conjugate impacts of electron withdrawing inductive effect and electron donating resonance effect of the chlorine substitutions, since the magnitude of relative contribution of these two effects for a particular chlorine substitution will be governed by its position on the aromatic benzene nucleus with respect to –OH/–COOH functional moiety [36].

However, the modifications of electronic charge distribution on the heavy atoms of TCSA as a result of electronic transition is indicative of the probability that the molecule attains a delocalized state on the excited surface which then relaxes to the K-form via transfer of the proton from –OH to –COOH moiety. The transition from ground to excited state is also found to produce no significant modification of dipole moment of TCSA (Table 2), a nice alignment of this result is reflected in experimental findings in terms of no notable dependency of the red shifted (PT) emission wavelength maxima upon medium polarity [9, 12, 15, 18, 25, 34].

*Potential Energy Surfaces: GSIPT and ESIPT Curves*

The photophysics of TCSA with special attention to ESIPT reaction can be best understood by investigating the potential energy surface (PES) along the PT reaction coordinate. This section thus deals with construction of the potential energy curves (PECs) utilizing the well-known "*distinguished coordinate*" approach [9, 12, 15, 25, 34] in which energy change is observed as a function of OH bond elongation, treated as the primary reaction coordinate [9, 12, 25, 30, 34]. The minimum-energy paths (MEPs) connecting the two structures in each electronic state are calculated to identify the major coordinates involved in the PT process and the results are displayed in Fig. 5. For the $S_0$ state all of the other degrees of freedom are relaxed without imposing any symmetry constraints. This was not possible or even desirable for the $S_1$ state (see "Computational procedures").

Analysis of the PECs in Fig. 5 reveals that the E-form represents the global minimum structure on the $S_0$ surface. The high instability of the K-form in the ground state coupled with the repulsive nature of the $S_0$ state-PEC dictates the nonviability of ground state intramolecular proton transfer (GSIPT) reaction in TCSA. The barrier height for a GSIPT reaction is ~0.3376 eV. At the same time, Fig. 5 exhibits the prominent diminution of the barrier height for PT reaction up on the $S_1$ surface, exploring its double-well nature. Thus Fig. 5 advocates for the inoperativeness of a GSIPT process in TCSA while simultaneously the feasibility of an ESIPT process is also indicated. These results are consistent with experimental findings and also are in track with literature reports [9, 12, 15, 18, 25, 30, 34]. Furthermore, it is fascinating to note that our theoretical computations do not deviate much from those including high-level calculations [28, 29], at least in respect of qualitative prediction of the nature of PES and the overall photophysics of the compound. Concerning the parent molecule SA, computation at the same level of theory negates a GSIPT process through a high energy barrier along $S_0$ PES with the E-form constituting the global minimum structure on $S_0$ surface. Whereas the occurrence of ESIPT in SA is dictated by considerable reduction of the barrier height for PT process on the $S_1$ PES, indeed the thermodynamic stabilities of the E- and K-forms are inverted on $S_1$ surface as a result of the ESIPT reaction (figures not given). Thus qualitative comparison of the PESs of TCSA with its parent molecule SA reveals commendable consistency regarding the business of ESIPT reaction and an overview of its photophysics. However, the impact of chlorine substitution on the phenomenon of ESIPT in SA is best criticized through a systematic comparison which reveals a progressively less favourable ESIPT along the sequence SA→5ClSA→3,5DCSA as explored in an increasing trend of energy-barrier to ESIPT i.e. ~0.018 eV in SA vs. ~0.022 eV in 5ClSA vs. ~0.024 eV in 3,5DCSA [23, 24]. While with TCSA being included in the sequence, a disruption of this trend is encountered. Figure 5 distinctly clarifies a barrierless proceeding of the transformation E*→K* and the result is rendered even more transparent upon inspection of Fig. 6 which presents a picturesque view of the barrierless cascade E*→K* (Fig. 6a and b depict the 3D PESs for $S_0$ and $S_1$ states towards ESIPT process in TCSA. As seen in the figure, the transformation from E- to K-form on the $S_0$-surface has to be passed through a transition state (TS) with high barrier energy. The E-form is located on a global minimum on $S_0$-surface. Whereas, quite a reverse pattern is reflected through the appearance of the $S_1$-surface, i.e., the stability of E- and K-forms (precisely E*- and K*-forms) are exchanged and the process of transformation faces a vanishingly small barrier.). This deviation of TCSA is an added evidence for the photophysics of the compound being somewhat modulated by the presence of chlorine substitutions as relative to its monochloro and dichloro counterparts. Now, as our experimental findings on the ESIPT reaction receive commendable assistance on the lexicon of theoretical computations, it is pertinent to mention at this stage that theoretical calculations with SA, 5ClSA [23] and 3,5DCSA [24] with the presently employed methods of calculations have proved creditable efficiency in correlating experimental findings.

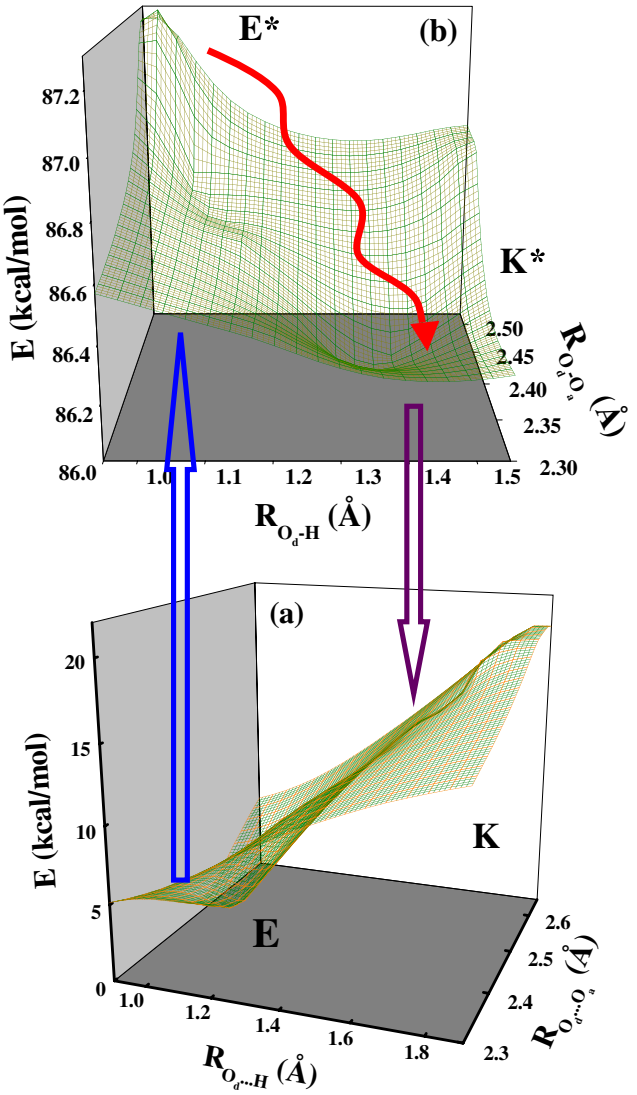


**Fig. 6** Three dimensional potential energy surfaces for the **a** ground and **b** excited states plotted as a function of $O_d$-H and $O_d$...$O_a$ distances for PT reaction in TCSA

Here it is necessary to establish the suitability of the presently employed computational methods for elucidating the ESIPT PESs in TCSA. In the following segment we present critical arguments for verification of our methods. Figures 7 reveal the variation of $O_d$...$O_a$ distance and angle ∠$O_d$...H...$O_a$ and $O_a$...H distance as a function of the PT reaction coordinate to show that apart from the O-H distance, the occurrence of PT involves significant deformation of the entire molecular architecture. As in case of $O_d$...$O_a$ distance, it contracts to a minimum and ∠$O_d$...H...$O_a$ increases to a maximum before relaxing to the K-form (Fig. 7a). This is indeed indicated by that the $S_0$ and $S_1$ surfaces are quite distinct with respect to their gross appearances and also that the $S_1$-surface minima are relatively shallow and located at a larger OH distance relative to $S_0$-surface minimum (Fig. 5). A crossover point between E- and K-forms is obtained at $R_{OH}$ ~ 1.3 Å (Fig. 7a). This mirror image plot stands in justification of the relaxed scan procedure for evaluation of PECs, as for otherwise a frozen calculation must have incorporated some obvious errors [15, 28, 30, 32, 34]. Figure 7b shows that the PT is dominated by a large change of distance between the two heteroatoms. The transfer mechanism can be described in three consecutive phases associated with the three regions, viz., E* minimum, barrier, K* minimum in the $S_1$ MEP energetics shown in Figs. 5 and 6. In the first phase the $O_d$...$O_a$ distance decreases (from 2.504 to 2.379 Å), along with a shortening of the $O_a$...H distance (from 1.612 to 1.146 Å), while the $O_d$-H bond is elongated much less (+0.30 Å). At the barrier the minimum in the $O_d$...$O_a$ distance is attained, and the $O_d$-H bond character is exchanged for $O_a$-H bond character. Finally, the heteroatoms separate again and the proton remains with $O_a$ [15].

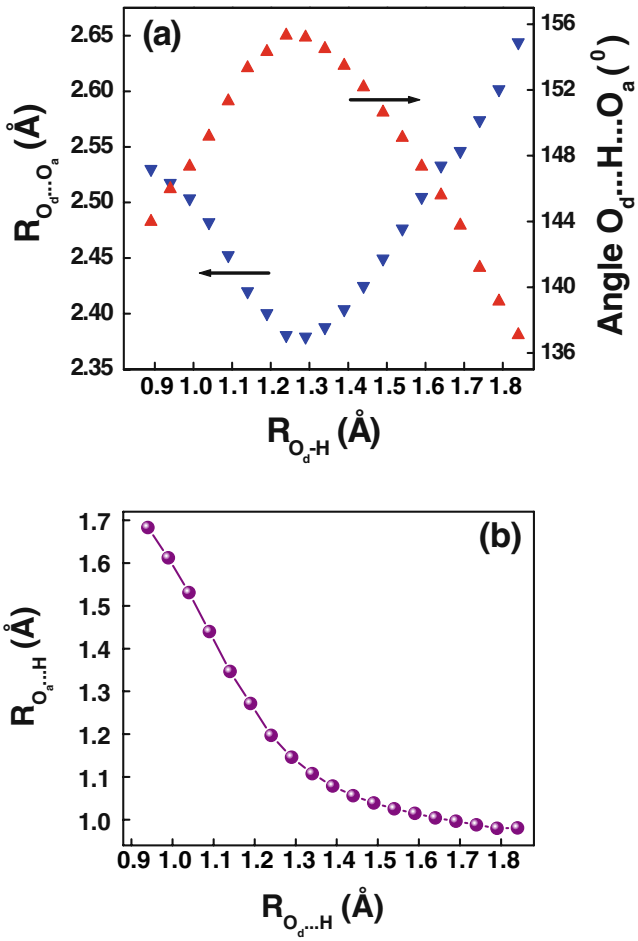


**Fig. 7** **a** Variation of $O_d$...$O_a$ distance and ∠$O_d$...H...$O_a$ angle, and **b** $O_a$...H distance with PT reaction coordinate, $O_d$-H distance in the $S_0$-state as calculated at DFT//B3LYP/6-311G** level

Upon excitation, the geometry E is conserved and deviates from E*. The temporal evaluation of the $S_1$ geometry starts from the FC-point (with the geometry of E), and when the system passes by the E* geometry, it has already gained considerable momentum, which is sufficient to carry TCSA over the small barrier to K* and thus allows ESIPT. The large gradient of PES at the FC point is the driving force that initiates ultrafast PT.

Variation of oscillator strength on traversing from E*- to the K*-from as a function of $R_{O\text{-}H}$ distance in the $S_1$ state (Fig. 8) supports high quantum yield of the K*-form (as seen in "Fluorescence quantum efficiency and excited state fluorescence lifetime") since the oscillator strength for K*-form is much higher in magnitude than that of the E*-form.

*Molecular Orbital Analysis*

The nodal plane concept of π-system molecular orbital to rationalize the phenomenon of ESIPT was first developed by Nagaoka and Nagashima and then the progress of time has witnessed a successful extension of the concept to various systems [38]. Analysis of the MOs shows that the HOMO is a π-orbital with bonding character primarily across $C_2$-$C_3$-$C_4$ bond and antibonding character across $C_3$-$O_d$ and $C_1$-$O_a$ bonds for both E- and K-forms. As observed in Fig. 9, HOMO of both E- and K-forms consists of a large electronic density projection over $O_d$-atom along with bonding character along $O_d$-H axis. Thus, transfer of the proton does not lead to any further stabilization through electronic redistribution. Whereas, the LUMO is of π* character and excitation of electron from HOMO to LUMO in the E-form leads to specific localization of the π-electron density over the IMHB ring with antibonding character along $C_3$-$O_d$ and $C_1$-$O_a$ bond axes. Transfer of proton in the excited state produces a LUMO in which the $O_a$-atom undergoes an enrichment of electronic density projection and a reduction of the same over $O_d$-atom. The presence of nodal plane between $C_3$-$O_d$ and $C_1$-$O_a$ bonds prevents electron delocalization involving the aromatic nucleus and thereby forbidding the reversal of proton transfer in the excited state [38–41].

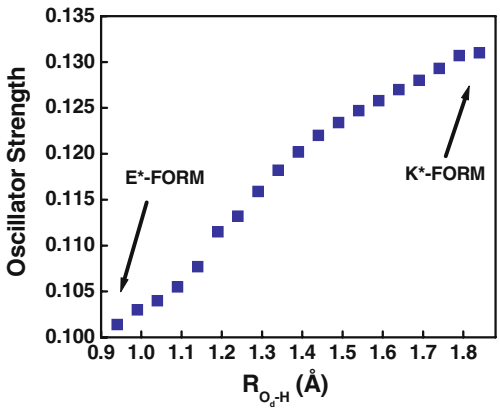


**Fig. 8** Variation of oscillator strength with PT reaction coordinate ($O_d$-H distance) in the $S_1$ state as computed at TDDFT/B3LYP/6-311G ** level

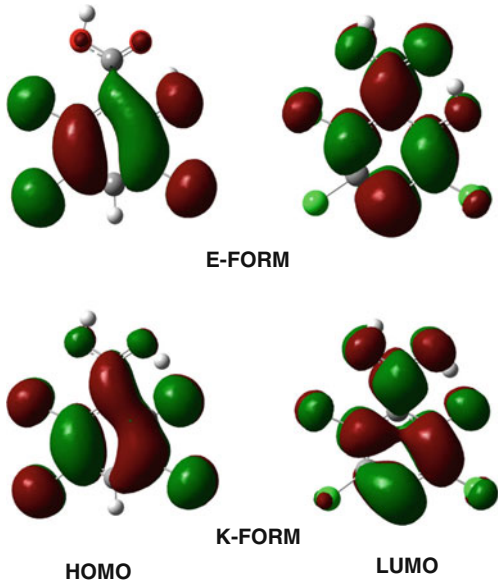


**Fig. 9** Molecular orbital pictures (HOMO-LUMO) of the E- and K-forms of TCSA as obtained from DFT//B3LYP/6-311G** level of calculation

*Evaluation of Intramolecular Hydrogen Bond Energy*

As seen in Fig. 10, DFT calculations yield energies for different conformations of TCSA produced by variation of torsional angle (θ) at the hydroxyl and carboxyl sites separately. The strength of IMHB ($E_{IMHB}$) for the A form (Chart 1) has been determined to be ~5.73 kcal/mol by rotating the phenolic OH group out of the H-bonded configuration and computing the energy difference between closed (E-form) and open forms (A-form) (Fig. 10a) [9, 12, 25, 34]. Similar calculation has been carried out by rotating the –COOH functional moiety and the strength of IMHB ($E_{IMHB}$) for R-form (Fig. 10b) is found to be ~4.23 kcal/mol. The difference in $E_{IMHB}$ seems to account for the presence of weak H-bonding interaction in the R-form [48]. Upon comparing the theoretically estimated IMHB energies for all four compounds the followings are the results: 11.63 in SA vs. 11.56 in 5ClSA vs. 8.75 in 3,5DCSA vs. 5.73 in TCSA for A-form (in kcal/mol) and 3.79 in SA vs. 3.85 in 5ClSA vs. 3.74 in 3,5DCSA vs. 4.23 in TCSA for R-form (in kcal/mol).

According to Zadorozhny and Ischenzo [49], the intramolecular hydrogen bond energy ($E_{IMHB}$) can be

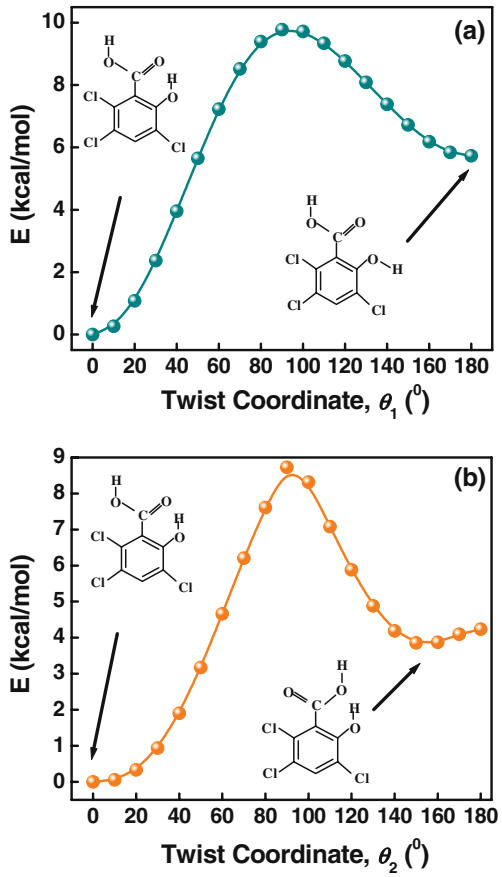


**Fig. 10** Variation of energy during the transformation **a** from E- to A-form of TCSA by twisting the angle $\theta_1$ and **b** from E- to R-form by twisting the angle $\theta_2$ (at DFT//B3LYP/6-311G** level of calculation). Twist coordinates $\theta_1$ and $\theta_2$ are as shown in chart 1

expressed by the relation: $\frac{\Delta\nu_{c=o}}{\nu_{c=o}} = -K_{C=O}E_{IMHB}$ where $\Delta\nu_{C=O}$ and $K_{C=O}$ are the magnitudes of the spectral shift and proportionality constant coefficient, respectively (reported value of $K_{C=O}=9.6\times10^{-4}$ mol-kJ$^{-1}$) [50]. Relative to the model compound benzoic acid ($\nu_{C=O}=1745$ cm$^{-1}$), red shift of the C = O stretching frequency in TCSA ($\Delta\nu=92$ cm$^{-1}$) signals the presence of IMHB interaction and the calculated value is found to be 13.86 kcal/mol. Thus unlike with SA, 5ClSA [23] and 3,5DCSA [24], the situation in TCSA becomes more cumbersome as is manifested through the lack of an acceptable harmony between theoretically and experimentally calculated IMHB energies. The experimentally obtained IMHB energies are: 12.28 in SA vs. 10.41 in 5ClSA vs. 11.81 in 3,5DSCA vs. 13.86 in TCSA (in kcal/mol), i.e. a relatively stronger IMHB is predicted in TCSA, which indeed, corroborates to the observation of minimum magnitude of barrier to ESIPT in TCSA, since the strength of IMHB puts its signature on ESIPT reaction on the way of ensuring a more favourable ESIPT with increasing IMHB energy. Nonetheless, that in the present case study with TCSA the discrepancy between experiments and theory is rendered most prominent might be a reflection of the simultaneous operation of several factors in governing the overall photophysical characteristics of the molecule, as is rigorously discussed above.

## Summary and Conclusion

The present work illustrates a detailed spectroscopic investigation in combination with theoretical calculations regarding the photophysics of a salicylic acid derivative-TCSA. Two absorption bands found in all solvents conform to the presence of two conformers of TCSA, namely the E- and R-forms, with simultaneous reflection of greater stability of the intramolecularly hydrogen bonded closed conformer (E-form). Fluorescence emission spectra in all solvents exhibit "*anomalous emission*" i.e. a distinct dual emission band for the R-form (~300 nm) and the K-form (~460–475 nm). The large Stokes shifted emission band is attributed to the PT form (K-form) generated as a result of ESIPT reaction across the pre-existing IMHB. The negligible sensitivity of the emission band for the PT form towards medium polarity complies with the intramolecular nature of the process.

The influence of the chlorine atoms on the photophysics of SA seems manifested through modulated IMHB energy, charge density distribution over the heavy atoms, ESIPT barrier in TCSA relative to SA. The photophysics of TCSA appears to be considerably complicated compared to the parent molecule SA and its monochloro (5ClSA) [23] and dichloro (3,5DCSA) [24] counterparts. However, the spectroscopic findings with all the four molecules (SA, 5ClSA, 3,5DCSA and TCSA) when brought under a single pavilion unravels some minor but detectable modulations as an outcome of chlorine substitution on the aromatic benzene nucleus. A conjugate impact of electron withdrawing inductive and electron donating resonance influences of the three chlorine atoms appears to play the pivotal role in governing the overall photophysics of the compound, apart from complicated solvent effects adding further complexities.

Quantum chemical calculations at DFT and HF levels have been successfully implemented to model the experimentally observed ESIPT phenomenon in TCSA, while at the same time, providing further insights to delve into the photophysics of the studied system. The E-form corresponds to the global minimum structure on the $S_0$ surface while the ESIPT curve for the first singlet excited state reflects two minima—for E* and K* forms together with an inversion in the stability pattern of the conformers and thereby predicting the operation of an ultrafast ESIPT in TCSA [41–45]. We are optimistic that

the detailed characterization of the photophysical properties of TCSA will augment further research with this potent ESIPT molecule on applicative arenas [46–47].

**Acknowledgements** BKP and AS gratefully acknowledge Council of Scientific and Industrial Research, New Delhi, India for research fellowships. NG acknowledges CSIR (Project no. 01(2161)07/EMR-II) and DST (Project no. SR/S1/PC/26/2008), Government of India, for financial supports. BKP greatly appreciates the cooperation received from Professor Soumen Basak, Chemical Sciences Division, Saha Institute of Nuclear Physics, Calcutta, India regarding the fluorescence lifetime measurements.

## References

1. Weller AH (1961) Fast reactions of excited molecules. Prog React Kinet 1:187
2. Chou PT, Martinez ML, Clements JH (1993) The observation of solvent-dependent proton-transfer/charge-transfer lasers form 4′-diethylamino-3-hydroxyflavone. Chem Phys Lett 204:395
3. (a) Chou PT, MxMorrow D, Aartsna TJ, Kasha M (1984) The proton-transfer laser. Gain spectrum and amplification of spontaneous emission of 3-hydroxyflavone. J Phys Chem 88:4596. (b) Park S, Kown OH, Kim S, Park S, Choi MG, Cha M, Park SY, Jang DJ (2005) Imidazole-based excited state intramolecular proton-transfer materials: Synthesis and amplified spontaneous emission from a large single crystal. J Am Chem Soc 127:10070.
4. Kim S, Park SY (2003) Photochemically gated protonation effected by intramolecular hydrogen bonding: towards stable fluorescence imaging in polymer films. Adv Matter 15:1341
5. Kim S, Seo J, Jung HK, Kim JJ, Park SY (2005) White luminescence from polymer thin films containing excited-state intramolecular proton-transfer dyes. Adv Matter 17:2077
6. Heller HJ, Blattmann HR (1972) Some aspects of the light protecting polymer. Pure Appl Chem 30:145
7. (a) Maity SS, Samanta S, Sardar PS, Pal A, Dasgupta S, Ghosh S (2008) Chem. Phys. (2008) Fluorescence, anisotropy and docking studies of proteins through excited state intramolecular proton transfer probe molecules. 354:162 (b) Sardar PS, Samanta S, Maity SS, Dasgupta S, Ghosh S (2008) Energy transfer photophysics from serum albumins to sequestered 3-hydroxy-2-naphthoic acid, an excited state intramolecular proton transfer probe. J Phys Chem B 112:3451. (c) Singh RB, Mahanta S, Guchhait N (2008) Study of interaction of proton transfer probe 1-hydroxy-2-naphthaldehyde with serum albumins: A spectroscopic study. J Photochem Photobiol B 91:1. (d) Singh RB, Mahanta S, Guchhait N (2008) Destructive and protective action of sodium dodecyl sulphate micelles on the native conformation of bovine serum albumin: A study by extrinsic fluorescence probe 1-hydroxy-2-naphthaldehyde. Chem Phys Lett 463:183. (e) Chakraborty B, Basu S (2009) Interaction of BSA with proflavin: A spectroscopic approach. J Lumin 129:34. (f) Zhong D, Douhal A, Zewail AH (2000) Femtosecond studies of protein-ligand hydrophobic binding and dynamics: Human serum albumin. Proc Natl Acad Sci, USA 97:14056 (g) Klymchenko AS, Shvadchak VV, Yushchenko DA, Jain N, Mely Y (2008) Excited state Intramolecular proton transfer distinguishes microenvironments in single- and double-stranded DNA. J Phys Chem B 112:12050
8. (a) Irie M (1994) Photoreactive material for ultra-high density optical memory. Elsevier, Amsterdam. (b) Lim SJ, Seo J, Park SY (2006) Photochromic switching of excited-state intramolecular proton-transfer (ESIPT) fluorescence: a unique route to high-contrast memory switching and nondestructive readout. J Am Chem Soc 128:14542
9. Maheshwari S, Chowdhury A, Sathyamurthy N, Mishra H, Tripathi PM, Chandrasekhar J (1999) Ground and excited state intramolecular proton transfer in salicylic acid: an ab initio electronic structure investigation. J Phys Chem A 103:6257
10. Mitsuzuka A, Fujii A, Ebata T, Mikami N (1998) Infrared spectroscopy of intramolecular hydrogen-bonded OH stretching vibrations in Jet-cooled methyl salicylate and its clusters. J Phys Chem A 102:9779
11. Acuna AU, Amat-Guerri F, Catalan J, Gonzalez-Tablas F (1980) Dual fluorescence and ground state equilibria in methyl salicylate, methyl 3-chlorosalicylate, and methyl 3-tert-butylsalicylate. J Phys Chem 84:629
12. (a) Mishra H, Maheshwary S, Tripathi HB, Sathyamurthy N (2005) An experimental and theoretical investigation of the photophysics of 1-hydroxy-2-naphthoic acid. J Phys Chem A 109:2746. (b) Sobolewski Al, Domcke W, Hattig C (2006) Photophysics of organic photostabilizers. Ab Initio study of the excited-state deactivation mechanisms of 2-(2'-Hydroxyphenyl) benzotriazole. J Phys Chem A 110:6301
13. Gora RW, Grabowski SJ, Leszczynski J (2005) Dimers of formic acid, acetic acid, formamide and pyrrole-2-carboxylic acid: an ab initio study. J Phys Chem A 109:6397
14. El-Nasr EAEA, Fujii A, Yahagi T, Ebata T, Mikami N (2005) Laser spectroscopic investigation of salicylic acids hydrogen bonded with water in supersonic jets: microsolvation effects for excited state proton dislocation. J Phys Chem A 109:2498
15. de Vivie-Riedle R, Waele VD, Kurtz L, Riedle E (2003) Ultrafast excited-sate proton transfer of 2-(2′-Hydroxyphenyl)benzothiazole: theoretical analysis of the skeletal deformations and the active vibrational modes. J Phys Chem A 107:10591
16. Organero JA, Moreno M, Santos L, Lluch JM, Douhal A (2000) Photoinduced proton transfer and rotational motion of 1-hydroxy-2-acetonaphthone in the $S_1$ state: a theoretical insights into its photophysics. J Phys Chem A 104:8424
17. Helmbrook LA, Kenny JE, Kohler BE, Scott GW (1983) Lowest excited singlet state of hydrogen-bonded methyl salicylate. J Phys Chem 87:280
18. Catalan J, de Paz JLG (2007) On the inoperativeness of the ESIPT process in the emission of 1-hydroxy-2-acetonaphthone: a reappraisal. J Phys Chem A 112:904
19. Lahmani F, Zehnacker-Rentien A (1997) Effect of substitution on photoinduced intramolecular proton transfer in salicylic acid. J Phys Chem A 101:6141
20. Rodriguez-Santiago L, Sodupe M, Oliva A, Berntran J (1999) Hydrogen atom or proton transfer in neutral and single positive ions of salicylic acid and related compounds. J Am Chem Soc 121:8882
21. Friedrich DM, Wang Z, Joly AG, Peterson KA, Callis PR (1999) Ground-state proton-transfer tautomer of the salicylate anion. J Phys Chem A 103:9644
22. (a) Pozdnyakov IP, Pigliucci A, Tkachenko N, Plyusnin VF, Vauthey E, Lemmetyinen H (2009) The photophysics of salicylic acid derivatives in aqueous solution. J Phys Org Chem 22:449. (b) Joshi HC, Gooijer C, van der Zwan G (2003) Substituion effects on the photophysical characteristics of the salicylic anion. J Fluoresc 13:227. (c) Kozma L, Hornak I, Eroshtak I, Nemet B (1990) Study of the fluorescent properties of salicylic acid derivatives in solutions. Z Prikladnoi Spektr 53:259
23. Paul BK, Samanta A, Guchhait N (2010) Deciphering the photophysica of 5-chlorosalicylic acid: evidence for excited state intramolecular proton transfer. Photochem Photobiol Sci 9:57
24. Paul BK, Samanta A, Guchhait N (2010) Influence of chlorine substitution on intramolecular hydrogen bond energy and ESIPT barrier: experimental and theoretical measurements on the photophysics of 3,5-dichlorosalicylic acid. J Mol Struct 977:78

25. Bisht P, Petek H, Yoshihara K, Nagashima U (1995) Excited state enol-keto tautomerization in salicylic acid: a supersonic free jet study. J Chem Phys 103:5290
26. (a) Muller A, O'Brien DF (2002) Supramolecular materals via polymerization of mesophases of hydrated amphiphiles. Chem Rev 102:727. (b) Janquera E, Aicart E (1999) Thermodynamic analysis of the binding of a hepatoprotectant drug, thioctic acid, by β-cyclodextrin. J Pharm Sci 88:626. (c) Park C, Youn H, Kim H, Noh T, Kook YH, Oh ET, Park HJ, Kim C (2009) Cyclodextrin-covered gold nanoparticles for targeted delivery of an anti-cancer drug. J Mater Chem 19:2310
27. (a) Mitra S, Das R, Mukherjee S (1998) Intramolecular proton transfer in inclusion complexes of cyclodextrins: role of water and highly polar nonaqueous meida. J Phys Chem B 102:3730 and references therein. (b) Sortino S, Giuffrida S, Fazio S, Monti S (2001) Spectroscopic characterization and photochemical behaviour of host-guest complexes between β-cyclodextrin and drugs containing biphenyl-like chromophore. New J Chem 25:707
28. (a) Foresman JB, Frisch Æ (1996) Exploring chemistry with electronic structure methods, 2nd ed. Gaussian, Inc., Pittsburgh, PA. (b) Frisch MJ et al (2003) Gaussian 03. Gaussian, Inc., Pittsburgh, PA
29. Palomar J, De Paz JLG, Catalan J (2000) Theoretical analysis of molecular structure, hydrogen bond strength, and proton transfer energy in O-H...O aromatic compounds. J Phys Chem A 104:6453
30. Tsai HHG, Sun HLS, Tan CJ (2010) TD-DFT study of the excited-state potential energy surface of 2-(2-hydroxyphenyl)benzimidazole and its amino derivatives. J Phys Chem A 114:4065
31. Shchavlev AE, Pankratov AN, Enchev V (2007) Intramolecular hydrogen-bonding interaction in 2-nitrosophenol and nitronaphthols: Ab Initio, density functional, and nuclear magnetic resonance theoretical study. J Phys Chem A 111:7112
32. (a) Singh RB, Mahanta S, Kar S, Guchhait N (2007) Photophysical properties of 1-hydroxy-2-naphthaldehyde: A combined fluorescence spectroscopy and quantum chemical calculations. Chem Phys 331:373. (b) Singh RB, Mahanta S, Kar S, Guchhait N (2008) Solvent dependent excited state spectral properties of 4-hydroxyacridine: evidence for only water mediated excited state proton transfer process. J Photochem Photobiol A 200:325
33. Lukeman M, Veale D, Wan P, Ranjit V, Munasinghe N, Corrie JET (2004) Photogeneration of 1, 5-naphthoquinone methides via excited-state (formal) intramolecular proton transfer (ESIPT) and photodehydration of 1-naphthol derivatives in aqueous solution. Can J Chem 82:240
34. Jeffrey GA (1997) An introduction to hydrogen bonding. Oxford University Press, USA
35. Catalan J, Mena E, Meutermans W, Elguero J (1992) Solvatochromism of a typical merocyanine: stilbazolium betaine and its 2,6-di-*tert*-butyl derivative. J Phys Chem 96:3645 and references therein
36. Sobolewski AL, Domcke W, Hattig C (2004) Intramolecular hydrogen bonding in the $S_1$ ($\pi\ \pi^*$) excited state of anthranilic acid and salicylic acid: TDDFT calculation of excited state geometries and infreared spectra. J Phys Chem A 108:10917
37. Mahanta S, Singh RB, Kar S, Guchhait N (2007) Excited state intramolecular proton transfer in 3-hydroxy-2-naphthaldehyde: a combined study by absorption and emission spectroscopy and quantum chemical calculation. Chem Phys 324:742
38. Nagaoka S, Nagashima U (1996) Effects of node of wave function upon excited-state intramolecular proton transfer of hydroxyanthraquinones and aminoanthraquinones. Chem Phys 206:353
39. Nagaoka S, Kusunoki J, Fujibuchi T, Hatakenaka S, Mukai K, Nagashima U (1999) Nodal-plane model of excited-state intramolecular proton transfer of 2-(*o*-hydroxyaryl)benzazoles. J Photochem Photobiol A 122:151
40. Nagaoka S, Nakamura A, Nagashima U (2002) Nodal-plane model for excited-state intramolecular proton transfer of *o*-hydroxybenzaldehyde: substituent effect. J Photochem Photobiol A 154:23
41. Mahanta S, Paul BK, Singh RB, Guchhait N (2010) Inequivalence of substitution pairs in hydroxynaphthaldehyde: a theoretical measurement by intramolecular hydrogen bond strength, aromaticity and excited-state intramolecular proton transfer reaction. J Comput Chem (in press)
42. Maliakal A, Lem G, Turro NJ, Ravichandran R, Suhadolnik JC, DeBellis AD, Wood MG, Lau J (2002) Twisted intramolecular charge transfer states in 2-arylbenzotriazoles: fluorescence deactivation via intramolecular electron transfer rather than proton transfer. J Phys Chem A 106:7680
43. Fluegge AP, Waiblinger F, Stein M, Keck J, Kramer HEA, Fischer P, Wood MG, DeBellis A, Ravichandran R, Leppard D (2007) Probing the intramolecular hydrogen bond of 2-(2-hydroxyphenyl)benzotriazoles in polar environment: a photophysical study of UV absorber efficiency. J Phys Chem A 111:9733
44. Martinez ML, Cooper WC, Chou PT (1992) A novel excited-state intramolecular proton transfer molecule, 10-hydroxybenzo[h]quinoline. Chem Phys Lett 193:151
45. Paul BK, Mahanta S, Singh RB, Guchhait N (2010) A DFT-based theoretical study on the photophysics of 4-hydroxyacridine: single-water-mediated excited state proton transfer. J Phys Chem A 114:2618
46. Paul BK, Guchhait N (2011) Constrained photophysics of an ESIPT probe within β-cyclodextrin nanocavity and chaotrope-induced perturbation of the binding phenomenon: implication towards hydrophobic interaction mechanism between urea and the molecular probe. J Colloid Interface Sci 353:237
47. Paul BK, Guchhait N (2010) Modulated photophysics of an ESIPT probe 1-hydroxy-2-naphthaldehyde within motionally restricted environments of liposome membranes having varying surface charges. J Phys Chem B 114:12528
48. Lakowicz JR (1999) Principles of fluorescence spectroscopy. Plenum, New York
49. Zadorozhny BA, Ischenzo IK (1965) Hydrogen bond energies and shifts of the stretching vibration bands of C = O groups. Opt Spectrosc (Engl Transl) 19:306
50. Tobita S, Yamamoto M, Kurahayashi N, Tsukagoshi R, Nakamura Y, Shizuka H (1998) Effects of electronic structures on the excited-state intramolecular proton transfer of 1-hydroxy-2-acetonaphthone and related compounds. J Phys Chem A 102:5206